APL Materials

Electrical and chemical analysis of Ti/Au contacts to β-Ga_2O_3

Cite as: APL Mater. **9**, 061104 (2021); https://doi.org/10.1063/5.0051340
Submitted: 24 March 2021 • Accepted: 10 May 2021 • Published Online: 04 June 2021

Luke A. M. Lyle, Tyson C. Back, Cynthia T. Bowers, et al.

Electrical and chemical analysis of Ti/Au contacts to β-Ga_2O_3

Cite as: APL Mater. 9, 061104 (2021); doi: 10.1063/5.0051340
Submitted: 24 March 2021 • Accepted: 10 May 2021 •
Published Online: 4 June 2021

Luke A. M. Lyle,[1,a] Tyson C. Back,[2] Cynthia T. Bowers,[2] Andrew J. Green,[3] Kelson D. Chabak,[3] Donald L. Dorsey,[2] Eric R. Heller,[2] and Lisa M. Porter[1]

AFFILIATIONS

[1] Department of Materials Science and Engineering, Carnegie Mellon University, Pittsburgh, Pennsylvania 15213, USA
[2] Air Force Research Laboratory Materials and Manufacturing Directorate, WPAFB, Dayton, Ohio 45433, USA
[3] Air Force Research Laboratory Sensors Directorate, WPAFB, Dayton, Ohio 45433, USA

[a] **Author to whom correspondence should be addressed:** llyle@andrew.cmu.edu

ABSTRACT

Chemical and electrical measurements of Ti/(010) β-Ga_2O_3 and Ti/(001) β-Ga_2O_3 interfaces were conducted as a function of annealing temperature using x-ray photoelectron spectroscopy (XPS), current density–voltage (J–V), and capacitance–voltage (C–V) measurements. XPS revealed partial Ti oxidation at both interfaces in the as-deposited condition, with more Ti oxidation on the (001) β-Ga_2O_3 epilayer surface than the (010) β-Ga_2O_3 substrate surface. The amount of oxidized Ti increased with annealing temperature. The Schottky barrier heights for as-deposited (unannealed) Au/Ti/(010) β-Ga_2O_3 and Au/Ti/(001) β-Ga_2O_3 contacts as determined from J–V and C–V measurements were between 0.64 and 0.83 eV. Shifts in XPS core level peaks for Ti/(010) β-Ga_2O_3 suggest that the Schottky barrier height decreases with temperature up to 350 °C for 10-min anneals and increases for 10-min anneals ≥460 °C. Taken together, the results suggest a strong dependence of Ti reactivity on the β-Ga_2O_3 surface, which can affect the electrical performance and stability of Ti/β-Ga_2O_3 ohmic contacts at elevated temperatures.

I. INTRODUCTION

Over the past decade, beta-gallium oxide (β-Ga_2O_3) has attracted intense interest as an ultrawide bandgap (~4.8 eV) semiconductor[1] due to its superior properties for high power electronic[2,3] and UV optoelectronic[4,5] devices, wide *n*-type doping range, and the availability of single-crystal melt-grown substrates. Furthermore, a variety of epitaxial growth methods have been demonstrated for β-Ga_2O_3, including halide vapor phase epitaxy (HVPE),[6–9] metalorganic chemical vapor deposition,[9–11] molecular beam epitaxy,[12,13] and pulsed laser deposition.[14,15]

The fabrication of low-resistance ohmic contacts is a necessary step for high power and high speed electronic/optoelectronic device development. The most common ohmic contacts for β-Ga_2O_3 comprise Ti/Au metallization annealed at 400–500 °C.[16,17] A few studies have examined the structural formation of the contact after the anneal by performing high-resolution transmission electron microscopy (HRTEM) and scanning transmission electron microscopy (STEM) imaging of the junction.[18–20] One such comprehensive study on (010) β-Ga_2O_3 attributes the ohmic mechanism to the formation of a ~5 nm Ti–TiO_x region partially lattice-matched to the substrate.[20] However, there is little literature of the as-deposited Ti/β-Ga_2O_3 interface and the characterization of the chemical and electrical properties of Ti/β-Ga_2O_3 junctions, and how they evolve as a function of annealing temperature is lacking.

The formation of metal oxides at the metal–semiconductor interface of β-Ga_2O_3 is important for future device applications. It has been established for Ti/Au contacts on (010) β-Ga_2O_3 that the Ti metal oxidizes when deposited.[19,20] In addition to Ti, Aller *et al.* demonstrated that a coherent α-Cr_2O_3 layer forms when Cr is deposited on (010) β-Ga_2O_3.[21] Furthermore, Hou *et al.* examined the electrical behavior of Pd/PdO_x/$(\bar{2}01)$ β-Ga_2O_3 contacts after high temperature device measurements (>300 °C).[22] These case studies of various metallizations to β-Ga_2O_3 indicate that

caution is needed when determining metal choices for device applications.

Studies of β-Ga_2O_3 surfaces and interfaces are a critical piece to optimize the material for high power applications. The low-symmetry of the monoclinic β-Ga_2O_3 structure suggests that different surface orientations can exhibit different properties (e.g., electrical properties[17,23–26]). X-ray photoelectron spectroscopy (XPS) characterization of $N_D = 4.5 \times 10^{18}$ cm^{-3} $(\bar{2}01)$ and $N_D = 6 \times 10^{18}$ cm^{-3} $(\bar{2}01)$ β-Ga_2O_3 bulk crystal surfaces has been examined by Gazoni *et al.* and Swallow *et al.*, respectively.[27,28] Gazoni *et al.* examined the effect of NaOH, H_2SO_4, and wet O_2 anneal surface treatments and the corresponding vacuum annealing on the surface band bending of $(\bar{2}01)$ β-Ga_2O_3. Experimentally, they determined that the bare samples were heavily depleted and exhibited upward band bending of ~1.0 eV, but when treated with NaOH, H_2SO_4 with an anneal at 600 °C, and a wet O_2 anneal at 600 °C, the band bending decreased.[27] Swallow *et al.* also examined the $(\bar{2}01)$ β-Ga_2O_3 surface and determined that the uncleaned $(\bar{2}01)$ surface is terminated with hydrogen, which produces surface donor states. Once the hydrogen is removed via *in situ* vacuum annealing, the bands bend upward ~0.5 eV relative to the H-terminated uncleaned surface.[28]

The (100) β-Ga_2O_3 bulk crystal surface was also examined. Lovejoy *et al.* found that highly doped (100) β-Ga_2O_3 crystals have flat bands near the surface, whereas nominally undoped, air-cleaved samples show upward band bending greater than 0.5 eV along with negatively charged surface defects. Navarro–Quezada *et al.* also found that for (100) β-Ga_2O_3, the bands bend upward ~0.5 eV.

In this study, we utilize an x-ray photoelectron spectroscopy (XPS) system with an *in situ* electron beam evaporator to deposit ~5 nm of Ti onto the surface of a (010) β-Ga_2O_3 substrate and a (001) β-Ga_2O_3 epilayer grown via halide vapor phase epitaxy (HVPE). XPS scans of the Ga 2p, O 1s, C 1s, Ti 2p, and valence band regions were acquired from the bare Ga_2O_3 surfaces and from the Ti/Ga_2O_3 junction as a function of various annealing temperatures between 150 and 670 °C. Additionally, Ti/Au (150/400 nm) Schottky diodes were fabricated on both (010) β-Ga_2O_3 and (001) β-Ga_2O_3 and annealed from 50 to 250 °C for 10 min each. Current density–voltage (J–V) and capacitance–voltage (C–V) measurements were conducted after each anneal and the diode properties were reported.

II. EXPERIMENTAL

Four Ga_2O_3 crystals purchased from Novel Crystal Technology were employed in this study: two *n*-type, Sn-doped (010) β-Ga_2O_3 substrates with doping concentration $N_D = 2 \times 10^{18}$ cm^{-3} and two *n*-type, Si-doped (001) β-Ga_2O_3 epilayers grown via halide vapor phase epitaxy (HVPE) with $N_D = 2 \times 10^{16}$ cm^{-3} grown on a (001) β-Ga_2O_3 substrate with $N_D = 2 \times 10^{18}$ cm^{-3}. For the XPS interface studies, a thin (~5 nm) layer of Ti was deposited on each Ga_2O_3 crystal using an electron-beam evaporator inside the XPS chamber. The pressure during deposition was ~3 to 5×10^{-10} Torr.

The XPS data were acquired with a Scienta Omicron standard Mg Kα (1253.6 eV) x-ray source and Argus hemispherical analyzer. The background pressure in the analysis chamber was $<3.0 \times 10^{-10}$ Torr. Samples were mounted on a flag style Mo sample holder and were heated from 150 to 670 °C for 10 min with a Ta filament mounted behind the Mo sample holder. The temperature was recorded with a pyrometer. High-resolution scans of the Ga 2p, O 1s, C 1s, Ti 2p, and valence band regions were acquired at 20 eV pass energy with 0.1 eV steps. Survey scans were acquired at 20 eV pass energy with 1.0 eV steps. The binding energy scale was calibrated against the Au $4f_{7/2}$ (84.0 eV) peak with an overall resolution of ~1 eV. The Ga 2p, O 1s, C 1s, and Ti 2p spectra were subtracted with a Shirley background and then fit using Gaussian and Lorentzian peak shapes for each chemical state in the region of interest. For the Ti 2p metal peaks, an additional asymmetry parameter was added to the Gaussian–Lorentzian convolution. The fitting procedure consisted of the z Levenberg–Marquardt routine that minimizes χ^2.

Scanning transmission electron microscopy (STEM) was performed on cross-sectional Ti/Ga_2O_3 samples to verify the Ti thickness of 5 nm using a Talos F-200X (FEI ThermoFisher Scientific) operated at an accelerating voltage of 200 kV. STEM imaging was performed by tilting to a zone axis and producing mass-thickness and phase contrast images. The Talos was operated in a scanning mode with a High Angle Annular Dark Field (HAADF) detector.

Ohmic contacts for electrical measurements were made by depositing Ti/Al/Ni/Au (20/100/50/50 nm) on the backside of the substrates via electron beam evaporation followed by a rapid thermal anneal (RTA) at 470 °C in N_2 for 1 min. Schottky contacts were deposited via electron beam evaporation utilizing a Ti/Au (150/400 nm) metallization to form vertical devices. Prior to deposition of both the ohmic and Schottky contacts, they were subject to a four-minute O_2 plasma exposure followed by acetone and isopropyl alcohol. Photoresist was removed using a hot (90 °C) Microposit 1165 organic solvent rinse (mixture of pure organic solvents) prior to the 4-min O_2 plasma exposure.

J–V measurements were obtained using an Agilent 4155C semiconductor parameter analyzer and a Signatone S-1160A-4N probe station. C–V measurements were performed at 1 MHz using an HP 4284 LCR meter and a Signatone S-1160A-4N probe station. In between J–V and C–V measurements, the samples were stored in a dry desiccator over the period of a month.

III. RESULTS

A. X-ray photoelectron spectroscopy

XPS survey scans of the bare surfaces of the (010) β-Ga_2O_3 substrate and (001) β-Ga_2O_3 epilayer, both in the as-received state, are shown in Fig. 1(a). Both survey spectra display only gallium, oxygen, and carbon peaks. The amount of dopants in the samples was well below the detection limit. The small C 1s peak is attributed to surface contamination from the air. *In situ* heating of the bare Ga_2O_3 surfaces to reduce the residual surface contamination was not conducted since this step is not typically conducted prior to Ti metallization during device fabrication.

Figure 1(b) shows the valence band spectra of the as-received (010) β-Ga_2O_3 substrate. The (001) Ga_2O_3 sample displayed evidence of charging due to its low doping level, and therefore, its valence band was not analyzed in this study. Using the typical method of a linear extrapolation of the valence band edge, the valence band maximum (VBM) for the (010) β-Ga_2O_3 sample is estimated to be 4.75 eV. However, Swallow *et al.* reported that linear extrapolation of the valence band edge in β-Ga_2O_3 causes an underestimation of the VBM by ~0.5 eV.[28] This phenomenon is attributed to the very low dispersion at the top of the valence band in β-Ga_2O_3

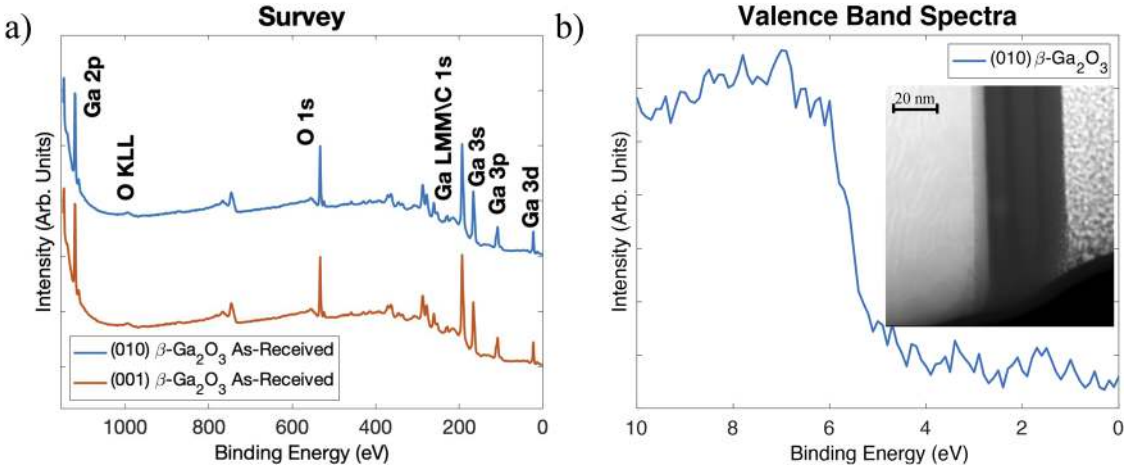

FIG. 1. (a) XPS survey scans of (010) βGa_2O_3 and (001) β-Ga_2O_3 and (b) valence band spectra of (010) β-Ga_2O_3 in the as-received state. Inset: HAADF-STEM image displaying cross section of the Ti/(010) Ga_2O_3 sample.

and its high effective mass, which cause a rapid onset in the density of states; in other words, the XPS instrumental broadening produces a lower slope (i.e., broadening) at the edge of the VB density of states than what is real. Due to the uncertainties in determining the VBM, we do not report absolute values of the band bending for the bare (010) β-Ga_2O_3 surface or of Schottky barrier heights determined from shifts in XPS core levels following the deposition of Ti. However, changes in core level peak positions are used to monitor relative changes in the Schottky barrier height of Ti/(010) β-Ga_2O_3 as a function of annealing temperature, as reported below.

XPS core level peaks were analyzed before and after deposition of Ti to investigate the surface and interfacial chemistry, respectively. O 1s and Ga $2p_{3/2}$ scans of the as-received (010) and (001) β-Ga_2O_3 surfaces are shown in Fig. 2. The Ga $2p_{3/2}$ and O 1s binding energies for the as-received (010) β-Ga_2O_3 sample were 1119.81 and 532.50 eV, respectively, in agreement with Ga $2p_{3/2}$ and O 1s core level energies for β-Ga_2O_3 in literature.[28] The O 1s peak for the (010) β-Ga_2O_3 bare surface was deconvolved into two separate peaks with FWHM = 1.50 eV, one centered at 532.50 eV and a minor peak centered at 533.90 eV. The main peak is ascribed to O bonded to Ga, whereas the minor peak is ascribed to OH adsorbed at the surface.[28] The O 1s peak for the (001) β-Ga_2O_3 bare surface was deconvolved into three separate peaks, each with FWHM = 1.50 eV: the main one centered at 533.14 eV and two minor ones at 534.64 and 530.44 eV. The main peak was fit to the expected O–Ga peak. [The shift from its position relative to the (010) surface is at least partially ascribed to charging in this sample.] The minor peaks at higher and lower binding energies were attributed to OH and C=O, respectively. The hydroxide composition of the O 1s spectra ($A_{OH} = \frac{A_{OH}}{A_{O1s}+A_{OH}}$) for (010) and (001) β-Ga_2O_3 as-received surfaces are estimated to be A_{OH} = 0.11 and 0.06, respectively. The C=O composition on the (001) β-Ga_2O_3 as-received surface is estimated to be $A_{C=O} = \frac{A_{C=O}}{A_{O1s}+A_{OH}+A_{C=O}} = 0.11$.

After deposition of 5 nm of Ti, the fitted peaks for C=O and OH were nearly or completely eliminated. This result suggests that the surface adsorbates are largely consumed by the Ti metal overlayer.

Figures 3 and 4 display scans of the Ti 2p peaks for the (010) and (001) β-Ga_2O_3 before (as-deposited) and after sequential 10-min anneals at 150, 250, and 350 °C. The corresponding fits for different oxidation states of Ti are also shown. The Ti $2p_{1/2}$ and $2p_{3/2}$ 0 oxidation states were fit using parameters extracted from the deposition of pure Ti metal in ultra-high vacuum conditions. The Ti $2p_{1/2}$ and Ti $2p_{3/2}$ + 4 oxidation states were fit using parameters extracted from the literature.[29–31] Peaks were assigned to the +3 oxidation state based on the residual fitting and literature values.[29–31] Additional details about the fitting procedures are provided in the supplementary material.

In Fig. 3(a), the as-deposited case, Ti/(010) β-Ga_2O_3, shows mostly metalized Ti with small contributions from Ti +3 and Ti +4 oxidation. After annealing [Figs. 3(b)–3(d)], the contributions from Ti oxidation increase with increasing annealing temperature. This result is not surprising since Ti is known to react readily with oxygen and is thermodynamically driven to reduce Ga_2O_3. This result demonstrates that titanium oxidation at the interface with (010) β-Ga_2O_3 occurs even with no annealing.

Interestingly, the Ti 2p spectrum for the Ti/(001) β-Ga_2O_3 as-deposited interface [Fig. 4(a)] shows significantly more oxidation than observed in the as-deposited Ti/(010) β-Ga_2O_3 interface. The oxidized-Ti component on the (001) Ga_2O_3 surface increased modestly with increasing annealing temperature. Bermudez[32] theoretically determined that the (010) β-Ga_2O_3 surface has a single surface configuration that is Ga- and O-terminated, whereas in the case of (001) β-Ga_2O_3, there are two separate surface configurations both O- terminated, with either singly or doubly unsaturated oxygen atoms. We calculated the atomic densities for the (010) and (001) surfaces of β-Ga_2O_3, and we estimate them to be 1.6×10^{15} and 2.3×10^{15} cm^{-2}. The higher atomic density on the (001) surface and the higher number of oxygen atoms at the (001) surface than the (010) surface likely contribute to the higher degree of Ti oxidation observed on the (001) orientation.

In principle, the Schottky barrier height of the Ti/β-Ga_2O_3 contact can be determined from XPS using the following equation:

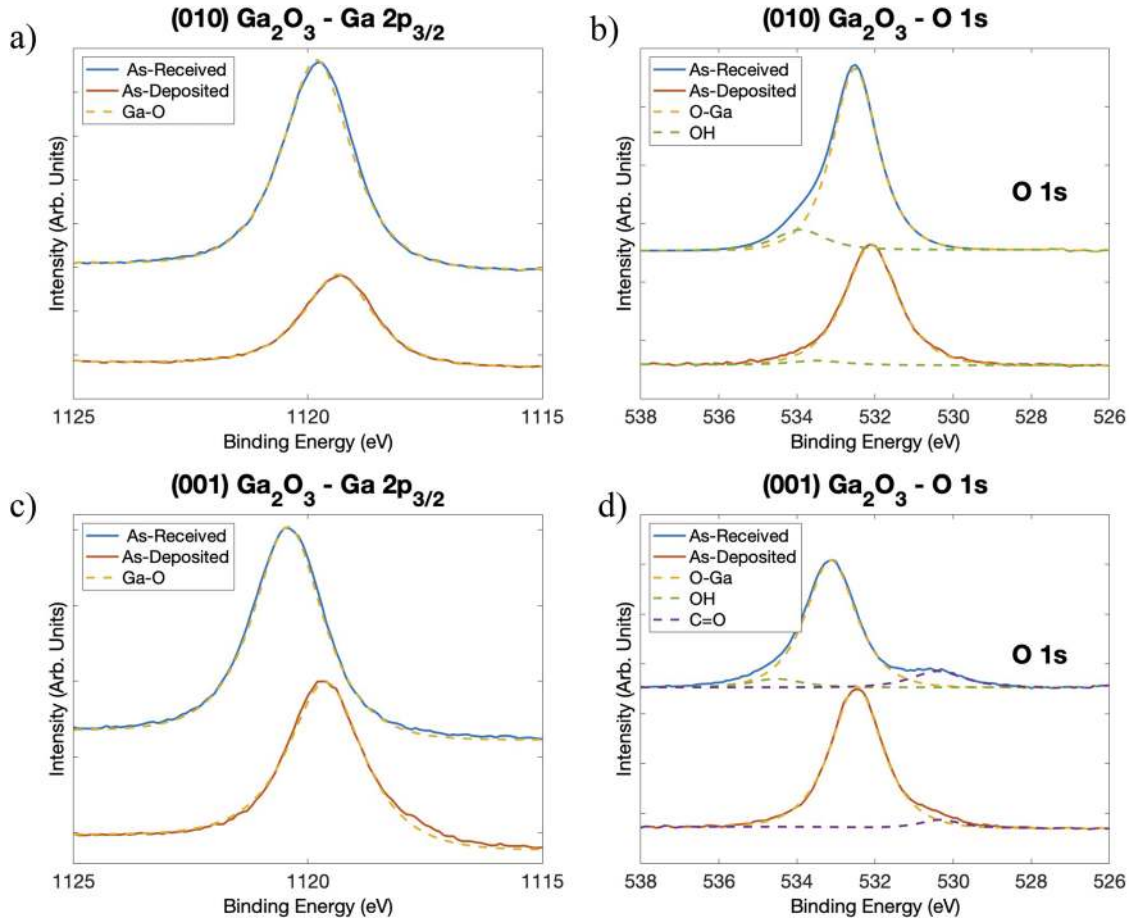

FIG. 2. (a) Ga $2p_{3/2}$ scan and (b) O 1s scan of (010) β-Ga_2O_3 in the as-received and as-deposited states. (c) Ga $2p_{3/2}$ scan and (d) O 1s scan of (001) β-Ga_2O_3 in the as-received and as-deposited states.

$$\phi_B^{XPS} = \left[E_{Ga_2p_{3/2}}^{Ga_2O_3} - E_V^{Ga_2O_3} + E_G\right] - E_{Ga_2p_{3/2}}^{Ti/Ga_2O_3}, \quad (1)$$

where $E_{Ga_2p_{3/2}}^{Ga_2O_3}$, $E_V^{Ga_2O_3}$, E_G, and $E_{Ga_2p_{3/2}}^{Ti/Ga_2O_3}$ refer to the binding energy of the Ga 2p $_{3/2}$ core level in Ga_2O_3 in the as-received state, the valence band maximum of the bare β-Ga_2O_3 surface, the bandgap of β-Ga_2O_3, and the binding energy of the Ga $2p_{3/2}$ core level after Ti deposition with or without an anneal, respectively. Due to the issues described previously regarding charging in the (001) sample and the error in determining the valence band maximum, the barrier height could not be directly computed from XPS measurements. However, the difference between the bare Ga $2p_{3/2}$ surface core level ($E_{Ga_2p_{3/2}}^{Ga_2O_3}$) and the Ga $2p_{3/2}$ core level after Ti deposition ($E_{Ga_2p_{3/2}}^{Ti/Ga_2O_3}$) was measured ($\Delta Ga2p_{3/2}$), and the values are listed in Table I. Because E_G and $E_V^{Ga_2O_3}$ are constants, the $\Delta Ga2p_{3/2}$ values represent relative changes in the barrier heights for different annealing conditions. The barrier height appeared to reach a minimum after the 10-min anneal at 350 °C. This result is consistent with experiments indicating optimized low-resistance ohmic contact formation for short (~1 min) anneals between 400–500 °C.[18]

The increase in $\Delta Ga_{2p3/2}$ at higher anneal temperatures indicates a corresponding increase in the Schottky barrier height. This result combined with the increased oxidation at higher temperatures points to a thermal stability issue with Ti contacts. It is yet to be determined to what extent the Ti/Al/Ni/Au ohmic contact scheme, which was used for the electrical measurements in this study, improves the contact stability for device operation at higher temperatures. This four-metal scheme is utilized to minimize the in- and out-diffusion during the annealing process.[33,34]

B. Current-voltage and capacitance-voltage measurements

To complement the XPS measurements, Au/Ti/β-Ga_2O_3 Schottky diodes were fabricated on both (010) and (001) β-Ga_2O_3 surfaces. J–V and C–V measurements at room temperature were performed before and after sequential 10-min anneals from 50 to 250 °C.

For Schottky contacts that follow the thermionic emission model, the current density (J) vs voltage (V) is expressed as

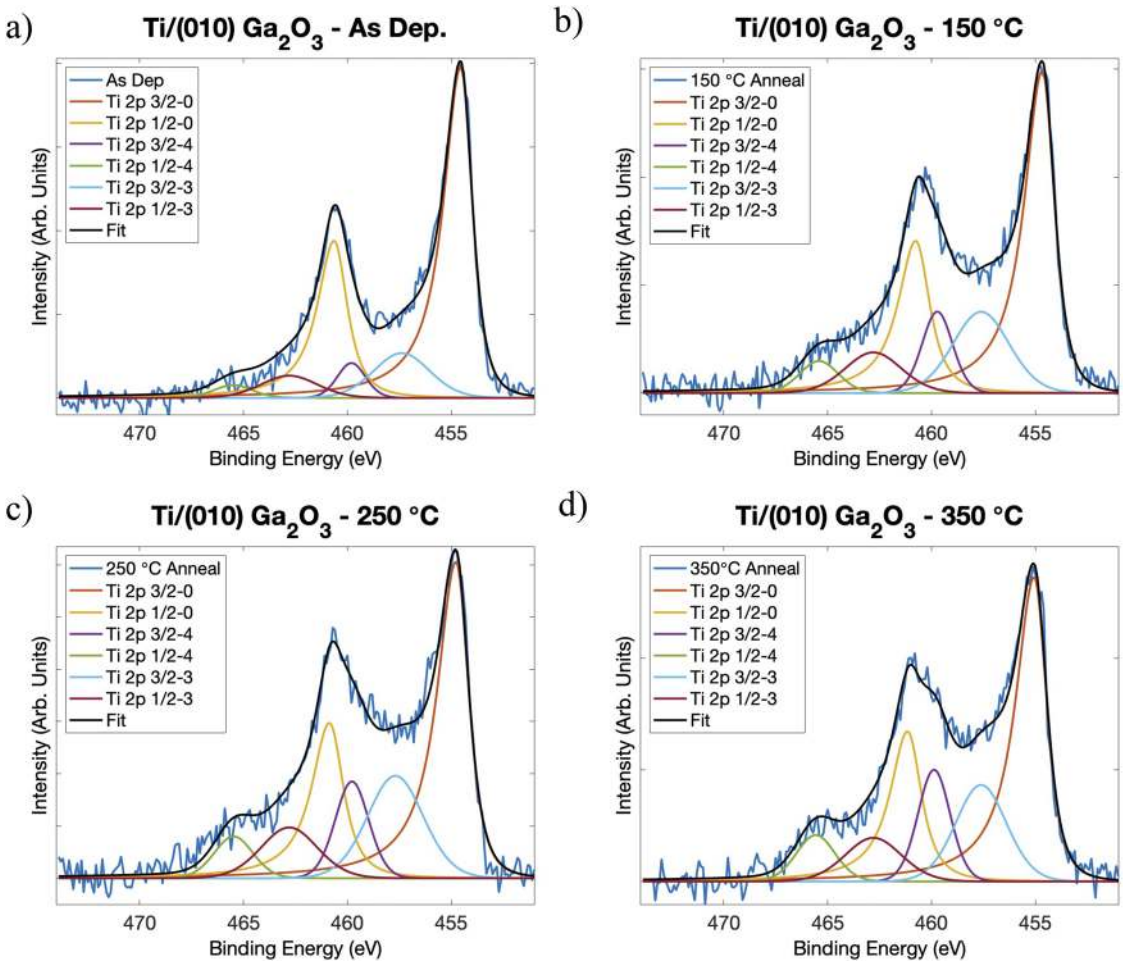

FIG. 3. Ti 2p spectra of Ti/(010) β-Ga_2O_3 (a) as-deposited and after sequential 10-min anneals at (b) 150 °C, (c) 250 °C, and (b) 350 °C.

$$J(V) = J_s\left[e^{\frac{q(V-IR_s)}{nkT}} - 1\right], \tag{2}$$

where q is the electronic charge, R_S is the series resistance, n is the ideality factor, and k is the Boltzmann constant. J_s is the saturation current density, given by

$$J_s = A^{**}T^2 e^{-\frac{q\phi_B^{JV}}{kT}}, \tag{3}$$

where A^{**} is the Richardson constant for the semiconductor and ϕ_B^{JV} is the J–V determined Schottky barrier height. The Richardson constant for β-Ga_2O_3 is reported to be 33.65 A/cm^{2}K^2[35] Ideality factors and Schottky barrier heights were calculated from J–V characteristics using the Cheung and Cheung method.[36] Figures 5(a) and 5(b) show the J–V plots for each Ga_2O_3 orientation. The average ideality factors of the Ti/Au contacts on (010) and (001) β-Ga_2O_3 were 1.08 and 1.12, respectively, in the as-deposited case. The J–V curves for the Au/Ti/(010) β-Ga_2O_3 diodes show linearity over four to five decades for all temperatures surveyed, whereas the diodes on (001) β-Ga_2O_3 were linear for only 2–3 decades of current. The reverse leakage currents for contacts on (010) β-Ga_2O_3 were approximately a factor of ten lower than the leakage currents on (001) β-Ga_2O_3 for the same temperature range. This difference could be due to a difference in the electrical quality of the (001) epilayer compared with the (010) substrate. The higher degree of Ti oxidation at the interface with (001) Ga_2O_3, as observed from our XPS measurements, could also play a role. Diodes on both surfaces display only small changes through annealing temperatures up to 150 °C. The diodes on both surfaces degraded following anneals above 150 °C to the extent that diodes on (010) Ga_2O_3 could no longer be measured.

Schottky barrier heights were also calculated from C–V measurements. For a Schottky diode under reverse bias, the capacitance can be expressed as[37]

$$\frac{A^2}{C(V)^2} = \frac{2\left(q\phi_B^{CV} - kT\ln\left(\frac{N_C}{N_d}\right) - qV - kT\right)}{q^2\varepsilon_s N_d}, \tag{4}$$

where ϕ_B^{CV}, ε_s, and N_d, are the C–V determined Schottky barrier height, semiconductor permittivity, and doping concentration,

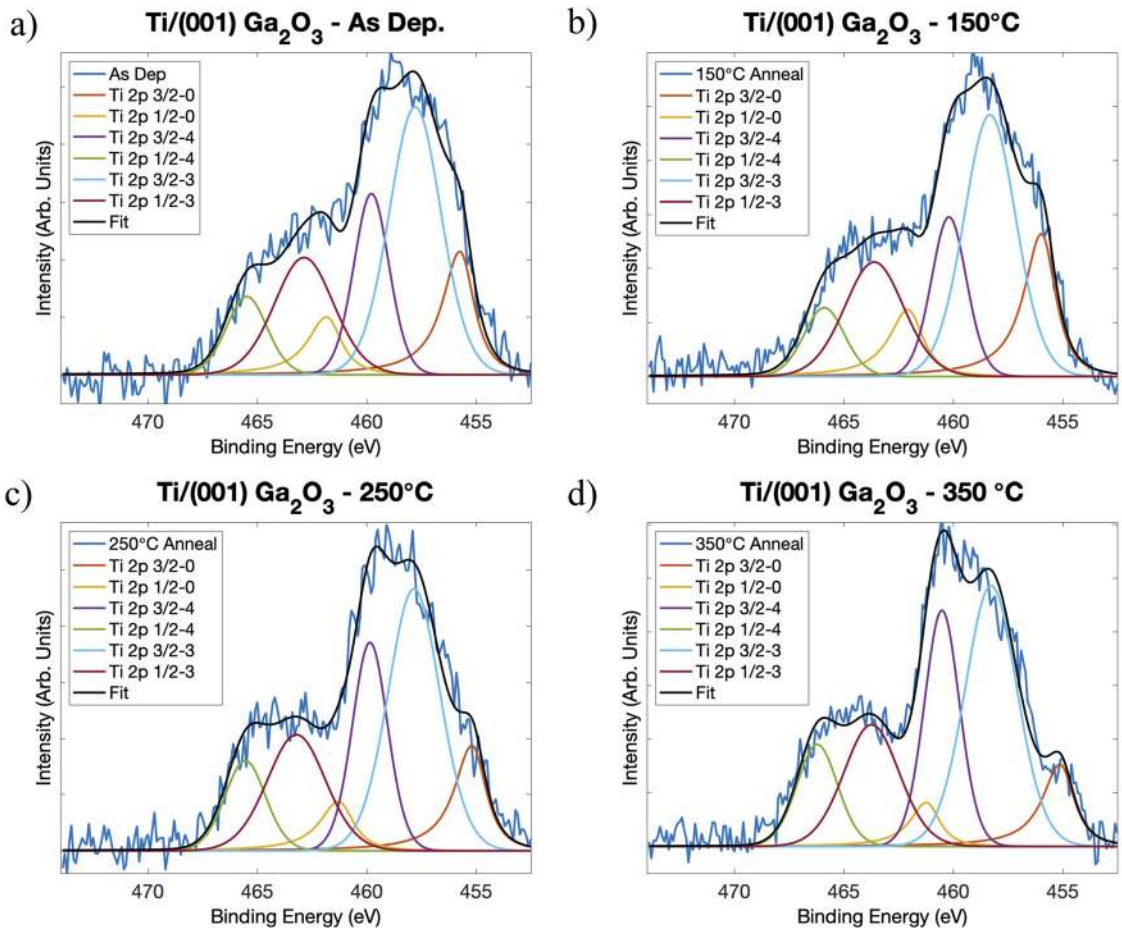

FIG. 4. Ti 2p spectra of Ti/(001) β-Ga_2O_3 (a) as-deposited and after sequential 10-min anneals at (b) 150 °C, (c) 250 °C, and (b) 350 °C.

TABLE I. Ideality factors and Schottky barrier heights determined from J–V and C–V measurements along with the peak shift of Ga $2p_{3/2}$ after deposition of the Ti metal for Ti/(010) and Ti/(001) $\beta-Ga_2O_3$ as a function of annealing temperature.

	Au/Ti/(010) β-Ga_2O_3				Au/Ti/(001) β-Ga_2O_3		
Annealing Temp. (°C)	n	$\phi^{IV}{}_B$ (eV)	$\phi^{CV}{}_B$ (eV)	$\Delta Ga2p_{3/2}$ (eV)	n	$\phi^{IV}{}_B$ (eV)	$\phi^{CV}{}_B$ (eV)
As-Dep.	1.08	0.64	0.82	0.50	1.12	0.49	0.83
50	1.06	0.70	0.94	···	1.15	0.48	0.70
100	1.08	0.68	0.95	···	1.15	0.49	0.74
150	1.07	0.68	0.90	0.49	1.14	0.48	0.74
200	···	···	···	···	1.21	0.44	0.64
250	···	···	···	0.41	1.24	0.40	0.46
350	···	···	···	0.26	···	···	···
460	···	···	···	0.69	···	···	···
560	···	···	···	1.19	···	···	···
670	···	···	···	1.19	···	···	···

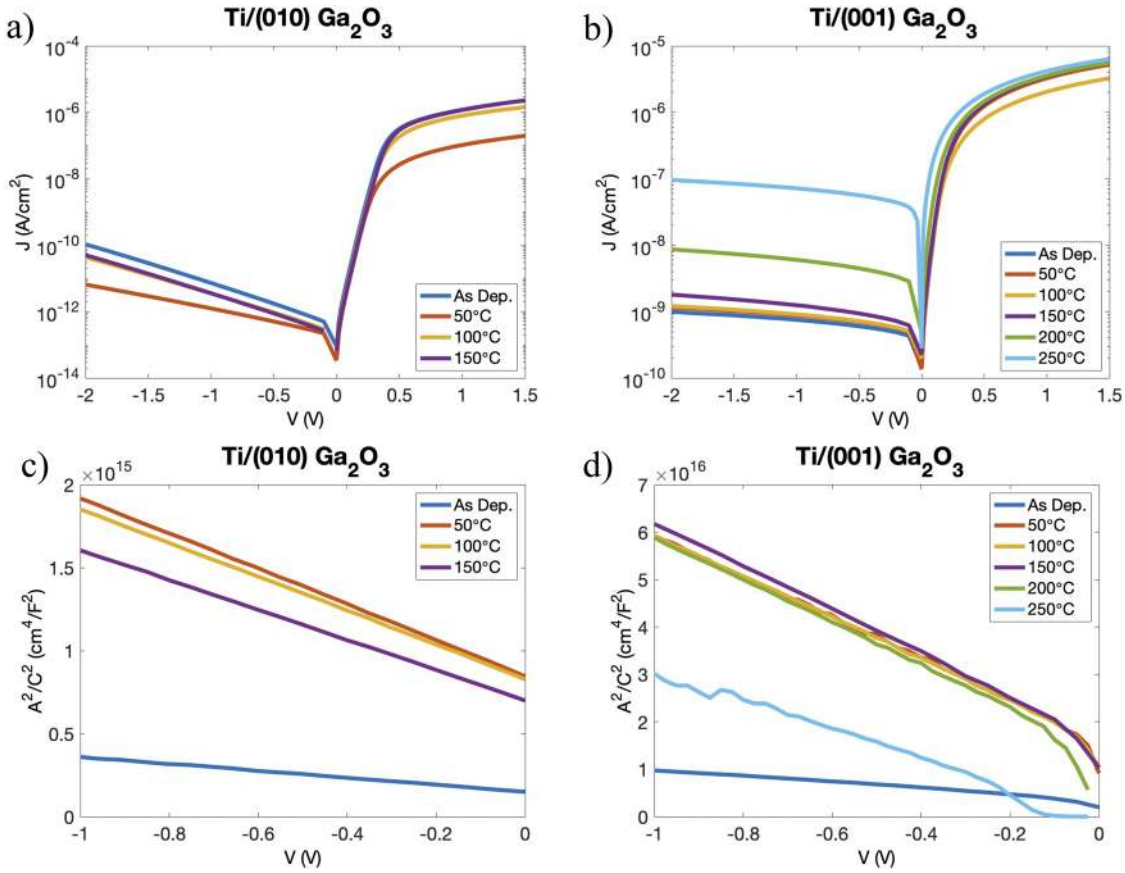

FIG. 5. J–V scans of (a) Ti/Au/(010) β-Ga_2O_3 contacts and (b) Ti/Au/(001) β-Ga_2O_3 contacts as a function of annealing temperature. (c) C–V scans of (c) Ti/Au/(010) β-Ga_2O_3 contacts and (d) Ti/Au/(001) β-Ga_2O_3 contacts as a function of annealing temperature.

respectively. Therefore, from a plot of A^2/C^2 vs V, N_d can be calculated from the slope and the barrier height can be calculated from the x-intercept.

A^2/C^2 vs V plots of the Au/Ti/(010) β-Ga_2O_3 diodes are uniformly linear, indicating a uniform doping density as a function of depth. A^2/C^2 vs V plots of the Au/Ti/(001) β-Ga_2O_3 diodes are linear at voltages above approximately −0.2 V but are nonlinear at lower voltages, an effect that is suspected to be due to an interfacial layer associated with the higher reactivity of this interface as observed from our XPS measurements.

J–V and C–V determined barrier heights are listed in Table I, along with ideality factors in the as-deposited state and after heating from 50 to 250 °C in air. The as-deposited J–V barrier heights for the Au/Ti/(010) and (001) β-Ga_2O_3 devices are 0.64 and 0.49 eV, whereas the C–V determined barrier heights for the as-deposited Au/Ti/(010) and (001) β-Ga_2O_3 devices are 0.82 and 0.83 eV.

After annealing up to 150 °C [the maximum anneal temperature for which the Ti/(010) β-Ga_2O_3 diodes were still conductive], the J–V and C–V determined barrier heights for both orientations change only modestly. J–V and C–V measurements of the Ti/(001) β-Ga_2O_3 diodes indicate that the barrier height begins to decrease above an annealing temperature of 200 °C. The Ti/(001) β-Ga_2O_3 diodes became too resistive to measure after annealing above 250 °C.

IV. CONCLUSIONS

This paper presents results of XPS, J–V, and C–V measurements of Ti contacts on (010) and (001) β-Ga_2O_3 as a function of annealing temperature. Significant differences in the chemical and electrical properties of the Ti/(010) β-Ga_2O_3 and Ti/(001) β-Ga_2O_3 interfaces were observed. Examples include differences in the degree of oxidation of the Ti contacts, i.e., larger amounts of Ti-oxidation observed on the (001) surface and larger J–V determined Schottky barrier heights on the (010) surface. The calculated C–V Schottky barrier heights were equivalent in the as-deposited state but differed after annealing; relative minima in the barrier heights for the (010) surface appeared after 10-min anneals at 350 °C. Changes in the barrier heights for higher temperature anneals and the increase in Ti-oxidation with increasing temperature indicate that Ti/Ga_2O_3 contacts are unstable at elevated temperatures. These results suggest that both orientational influences of structurally anisotropic β-Ga_2O_3 can have strong chemical effects on metal–semiconductor

contacts and that Ti-based electrical contacts degrade quickly under high temperature operation.

ACKNOWLEDGMENTS

This material is based upon work supported by the Air Force Office of Scientific Research (Program Manager, Dr. Ali Sayir) under Award No. FA9550-18-1-0387. The authors would like to thank Don Baer and Mark Engelhard at the Environmental Molecular Sciences Laboratory at PNNL for helpful discussions regarding XPS analysis and Don Dorsey at the Air Force Research Laboratory for coordinating joint CMU-AFRL research.

DATA AVAILABILITY

The data that support the findings of this study are available from the corresponding author upon reasonable request.

REFERENCES

[1]C. Janowitz, V. Scherer, M. Mohamed, A. Krapf, H. Dwelk, R. Manzke, Z. Galazka, R. Uecker, K. Irmscher, R. Fornari, M. Michling, D. Schmeißer, J. R. Weber, J. B. Varley, and C. G. V. D. Walle, New J. Phys. **13**, 085014 (2011).
[2]M. Higashiwaki, K. Sasaki, A. Kuramata, T. Masui, and S. Yamakoshi, Appl. Phys. Lett. **100**, 013504 (2012).
[3]K. D. Chabak, K. D. Leedy, A. J. Green, S. Mou, A. T. Neal, T. Asel, E. R. Heller, N. S. Hendricks, K. Liddy, A. Crespo, N. C. Miller, M. T. Lindquist, N. A. Moser, R. C. Fitch, D. E. Walker, D. L. Dorsey, and G. H. Jessen, Semicond. Sci. Technol. **35**, 013002 (2020).
[4]L. A. M. Lyle, S. Okur, V. S. N. Chava, M. L. Kelley, R. F. Davis, G. S. Tompa, M. V. S. Chandrashekhar, A. B. Greytak, and L. M. Porter, J. Electron. Mater. **49**(6), 3490–3498 (2020).
[5]Y. Xu, X. Chen, D. Zhou, F. Ren, J. Zhou, S. Bai, H. Lu, S. Gu, R. Zhang, Y. Zheng, and J. Ye, IEEE Trans. Electron Devices **66**, 2276–2281 (2019).
[6]M. Baldini, M. Albrecht, A. Fiedler, K. Irmscher, R. Schewski, and G. Wagner, ECS J. Solid State Sci. Technol. **6**, Q3040 (2016).
[7]H. Murakami, K. Nomura, K. Goto, K. Sasaki, K. Kawara, Q. T. Thieu, R. Togashi, Y. Kumagai, M. Higashiwaki, A. Kuramata, S. Yamakoshi, B. Monemar, and A. Koukitu, Appl. Phys. Express **8**, 015503 (2015).
[8]V. I. Nikolaev, A. I. Pechnikov, S. I. Stepanov, I. P. Nikitina, A. N. Smirnov, A. V. Chikiryaka, S. S. Sharofidinov, V. E. Bougrov, and A. E. Romanov, Mater. Sci. Semicond. Process. **47**, 16–19 (2016).
[9]Y. Yao, S. Okur, L. A. M. Lyle, G. S. Tompa, T. Salagaj, N. Sbrockey, R. F. Davis, and L. M. Porter, Mater. Res. Lett. **6**, 268 (2018).
[10]Y. Yao, L. A. M. Lyle, J. A. Rokholt, S. Okur, G. S. Tompa, T. Salagaj, N. Sbrockey, R. F. Davis, and L. M. Porter, ECS Trans. **80**, 191–196 (2017).
[11]C. Joishi, S. Rafique, Z. Xia, L. Han, S. Krishnamoorthy, Y. Zhang, S. Lodha, H. Zhao, and S. Rajan, Appl. Phys. Express **11**, 031101 (2018).
[12]Y. Oshima, E. Ahmadi, S. C. Badescu, F. Wu, and J. S. Speck, Appl. Phys. Express **9**, 061102 (2016).
[13]T. J. Asel, E. Steinbrunner, J. Hendricks, A. T. Neal, and S. Mou, J. Vac. Sci. Technol. A **38**, 043403 (2020).
[14]K. D. Leedy, K. D. Chabak, V. Vasilyev, D. C. Look, J. J. Boeckl, J. L. Brown, S. E. Tetlak, A. J. Green, N. A. Moser, A. Crespo, D. B. Thomson, R. C. Fitch, J. P. McCandless, and G. H. Jessen, Appl. Phys. Lett. **111**, 012103 (2017).
[15]K. D. Leedy, K. D. Chabak, V. Vasilyev, D. C. Look, K. Mahalingam, J. L. Brown, A. J. Green, C. T. Bowers, A. Crespo, D. B. Thomson, and G. H. Jessen, APL Mater. **6**, 101102 (2018).
[16]K. Jiang, L. A. M. Lyle, E. Favela, D. Moody, T. Lin, K. K. Das, A. Popp, Z. Galazka, G. Wagner, and L. M. Porter, ECS Trans. **92**, 71–78 (2019).
[17]Y. Yao, R. Gangireddy, J. Kim, K. K. Das, R. F. Davis, and L. M. Porter, J. Vac. Sci. Tech. B **35**, 03D113 (2017).
[18]Y. Yao, R. F. Davis, and L. M. Porter, J. Electron. Mater. **46**, 2053–2060 (2016).
[19]M.-H. Lee and R. L. Peterson, ECS J. Solid State Sci. **8**, Q3176–Q3179 (2019).
[20]M.-H. Lee and R. L. Peterson, APL Mater. **7**, 022524 (2019).
[21]H. T. Aller, X. Yu, A. Wise, R. S. Howell, A. J. Gellman, A. J. H. McGaughey, and J. A. Malen, Nano Lett. **19**, 8533–8538 (2019).
[22]C. Hou, R. M. Gazoni, R. J. Reeves, and M. W. Allen, IEEE Trans. Electron Devices **68**(4), 1791–1797 (2021).
[23]L. A. M. Lyle, L. Jiang, K. K. Das, and L. M. Porter, in *Gallium Oxide: Technology, Devices and Applications*, edited by S. J. Pearton, F. Ren, and M. A. Mastro (Elsevier, 2019), p. 231.
[24]E. Farzana, Z. Zhang, P. K. Paul, A. R. Arehart, and S. A. Ringel, Appl. Phys. Lett. **110**, 202102 (2017).
[25]L. A. M. Lyle, Ph.D. dissertations (Carnegie Mellon University; ProQuest Publishing, 2020), p. 28094822.
[26]L. A. M. Lyle, K. Jiang, E. V. Favela, K. Das, A. Popp, Z. Galazka, G. Wagner, and L. M. Porter, J. Vac. Sci. Tech. A **39**, 033202 (2021).
[27]R. M. Gazoni, L. Carroll, J. I. Scott, S. Astley, D. A. Evans, A. J. Downard, R. J. Reeves, and M. W. Allen, Phys. Rev. B **102**, 035304 (2020).
[28]J. E. N. Swallow, J. B. Varley, L. A. H. Jones, J. T. Gibbon, L. F. J. Piper, V. R. Dhanak, and T. D. Veal, APL Mater. **7**, 022528 (2019).
[29]C. F. Chang, T. C. Koethe, Z. Hu, J. Weinen, S. Agrestini, L. Zhao, J. Gegner, H. Ott, G. Panaccione, H. Wu, M. W. Haverkort, H. Roth, A. C. Komarek, F. Offi, G. Monaco, Y. F. Liao, K. D. Tsuei, H. J. Lin, C. T. Chen, A. Tanaka, and L. H. Tjeng, Phys. Rev. X **8**, 021004 (2018).
[30]P. S. Bagus, C. J. Nelin, C. R. Brundle, and S. A. Chambers, J. Phys. Chem. C **123**, 7705–7716 (2018).
[31]S. A. Chambers, M. H. Engelhard, L. Wang, T. C. Droubay, M. E. Bowden, M. J. Wahila, N. F. Quackenbush, L. F. J. Piper, T.-L. Lee, C. J. Nelin, and P. S. Bagus, Phys. Rev. B **96**, 205143 (2017).
[32]V. M. Bermudez, Chem. Phys. **323**, 193–203 (2006).
[33]N. A. Blumenschein, T. Moule, S. Dalcanale, E. Mercado, M. Singh, J. W. Pomeroy, M. Kuball, G. Wagner, T. Paskova, J. F. Muth, K. D. Chabak, N. A. Moser, G. H. Jessen, E. R. Heller, N. C. Miller, A. J. Green, A. Popp, A. Crespo, K. Leedy, and M. Lindquist, IEEE Trans. Electron Devices **67**, 204–211 (2020).
[34]K. D. Chabak, N. Moser, A. J. Green, D. E. Walker, S. E. Tetlak, E. Heller, A. Crespo, R. Fitch, J. P. McCandless, K. Leedy, M. Baldini, G. Wagner, Z. Galazka, X. Li, and G. Jessen, Appl. Phys. Lett. **109**, 213501 (2016).
[35]S. J. Pearton, J. Yang, P. H. Cary, F. Ren, J. Kim, M. J. Tadjer, and M. A. Mastro, Appl. Phys. Rev. **5**, 011301 (2018).
[36]S. K. Cheung and N. W. Cheung, Appl. Phys. Lett. **49**, 85–87 (1986).
[37]S. M. Sze and K. N. Kwok, Phys. Semicond. Devices **763**, 763 (2007).